Monatsh Chem (2010) 141:259–267
DOI 10.1007/s00706-010-0250-3

ORIGINAL PAPER

Friedel–Crafts acylation of toluene using superacid catalysts in a solvent-free medium

E. A. El-Sharkawy · Shar S. Al-Shihry

Received: 20 May 2009 / Accepted: 1 January 2010 / Published online: 16 February 2010

Abstract Sulfated tin oxide and sulfated zirconia containing different amounts of sulfate and Al_2O_3-sulfated zirconia catalysts were prepared. The materials were characterized by DTA/TGA/DTG, XRD, FT-IR, and BET surface-area techniques. Surface acidity was determined using TGA of pyridine-pretreated samples, and acid strength was determined by potentiometric titration of the solid catalysts with *n*-butylamine in non-aqueous media. The catalytic activity of prepared samples was tested by Friedel–Crafts acylation of toluene with acetic acid anhydride. Incorporation of sulfate into SnO_2 impedes sintering and is associated with a decrease of surface area. Sulfated tin oxide has greater acidity and higher acid strength than Al^{3+}-impregnated sulfated zirconia, giving, therefore, a higher yield of acylation products. Sulfated tin oxide was found to pass through maxima of higher acidity and higher efficiency for the acylation reaction when sulfate loading is 10 wt%. A good relationship between structural characteristics, acidity, and catalytic activity is observed.

Keywords Sulfated tin oxide · Zirconia · Friedel–Crafts · Acylation · Toluene · Acidity

E. A. El-Sharkawy · S. S. Al-Shihry
Chemistry Department, College of Science,
King Faisal University, P. O. Box 400,
Hofuf 31982, Saudi Arabia

E. A. El-Sharkawy (✉)
Chemistry Department, College of Education at Al-Ariesh,
Suez Canal University, Ismailia, Egypt
e-mail: easharkawy@yahoo.com

Introduction

Friedel–Crafts acylation of aromatic compounds is the most important reaction for the fabrication of raw materials for several industrial applications from petrochemical to pharmaceutical [1, 2]. In general, metal halides ($AlCl_3$, $FeCl_3$, etc.) or strong mineral acids (e.g., HF) are used as catalysts for aromatic acylation. However, use of homogeneous catalysts is associated with environmental problems, e.g., production of hazardous corrosive waste products. Therefore, great efforts have been devoted to replacing homogeneous catalysts with recoverable and regenerable solid catalysts [3–5].

Supported or unsupported superacid catalysts are well investigated in catalyzed reactions, e.g., esterification [6–8], skeletal isomerization [9–12], alkylation–acylation [13–17], and cracking reactions [6, 18]. Many solid acids, supported or unsupported, have been reported, including SO_4^{2-}/ZrO_2/MCM-41 [19–22], perfluorinated Nafion/SBA-15 [23, 24], heteropoly acids/MCM-41 [25], sulfated metal oxides [26, 27], and borate zirconia [28]. Such catalysts are classified as strong Bronsted acids and behave similarly to mineral acids (H_2SO_4, HF, HNO_3) [29–31].

Sulfated tin oxide is one candidates for the strongest surface acidity. The acid strength of sulfated tin oxide is reported to be higher than that of sulfated zirconia [32, 33]. Nevertheless, there have been few papers on sulfated tin oxide catalysts because of difficulty in preparation compared with the relative ease of preparation for SO_4^{2-}/ZrO_2. Depending on the preparation conditions, the active acid sites of sulfated metal oxides consist of polysulfate species comprising three or four oligomers with two ionic S–O−M bonds in addition to coordination bonds of S=O with M [34]. Determination of surface acidity remains an urgent task in acid-catalyzed reactions and can be carried out

using various techniques, including titration of catalysts with *n*-butylamine in the presence of Hammett indicators [35, 36], microcalorimetric methods and infrared spectroscopy [37, 38], temperature-programmed desorption (TPD) of adsorbed bases [28, 39], using of DTA and TGA [40, 41], and poisoning of acid centers with some organic bases [42, 43].

Because use of SO_4^{2-}/SnO_2 in Friedel–Crafts reactions has received a little attention [44], in this research they have been compared with SO_4^{2-}/ZrO_2 and Al^{3+}-incorporated SO_4^{2-}/ZrO_2. Our objectives in this study were the use of prepared SO_4^{2-}/SnO_2 in Friedel–Crafts acylation of toluene, comparison of the catalytic activity of SO_4^{2-}/SnO_2 with that of SO_4^{2-}/ZrO_2 and Al^{3+}-incorporated SO_4^{2-}/ZrO_2, and determination of the surface acidity using simple reported methods [45, 46], the textural characteristics, and the structural characteristics of the catalysts, and the effect of these variables on acylation efficiency.

Results and discussion

Thermal analysis

DTA of sulfated $Zr(OH)_4$ containing 20 wt% SO_4^{2-} (Fig. 1) furnishes a broad and overlapped endotherm when the temperature is below 220 °C. This may be attributed to evolution of adsorbed water and the dehydroxylation of $Zr(OH)_4$. Two weak endotherms centered at 296 and 467 °C may arise from the complete dehydroxylation of $Zr(OH)_4$ to ZrO_2 and removal of SO_4^{2-} groups; no appreciable weight loss is observed. Moreover, DTA/TGA curves contain an exothermic peak at 552 °C, corresponding to a constant-weight region in the TG curve, and indicates the formation of a crystalline phase from the amorphous precursor (Fig. 1) [47, 48]. Scurrell and Srinivasan pointed out that introduction of sulfate into ZrO_2 gives the latter exotherm and inhibits its crystallization [47, 48], so that the decrease in S_{BET}-N_2 on addition of Al^{3+}-sulfated ZrO_2 becomes less pronounced.

The DTA curve of Al/SZ (Fig. 2) has a different shape, including three sharp endotherms at 99, 181, and 237 °C, with an extra, weak, endotherm at 468 °C. These endotherms correspond to four areas of weight loss as depicted in the TG curves. The peak located at 99 °C may be attributed to removal of adsorbed water, and dehydroxylation of $Zr(OH)_4$ occurs at 273 °C. The sharp endotherm assigned at 181 °C may be related to the formation of Al_2O_3.

Figure 3 shows DTA/TGA/DTG of SO_4^{2-}-impregnated $Sn(OH)_4$. The TGA curve is indicative of weight loss of 6.44% below 200 °C, which corresponds to the DTA endotherm related to the removal of physisorbed water, whereas the second endotherm located at 257 °C may be attributed to the overlapped process of bond fission of M–sulfate groups and the removal of acetate ions used in the washing solution [33]. The exothermic peak at 586 °C is attributed to crystallization of the tin oxide [49], without a pronounced weight loss. The curve contains a second region of weight loss of 7%, where the exothermic process is shifted to higher temperature. This indicates that interaction of surface sulfate with the amorphous phase stabilizes the amorphous nature and shifts the crystallization to higher temperatures [12, 49, 50].

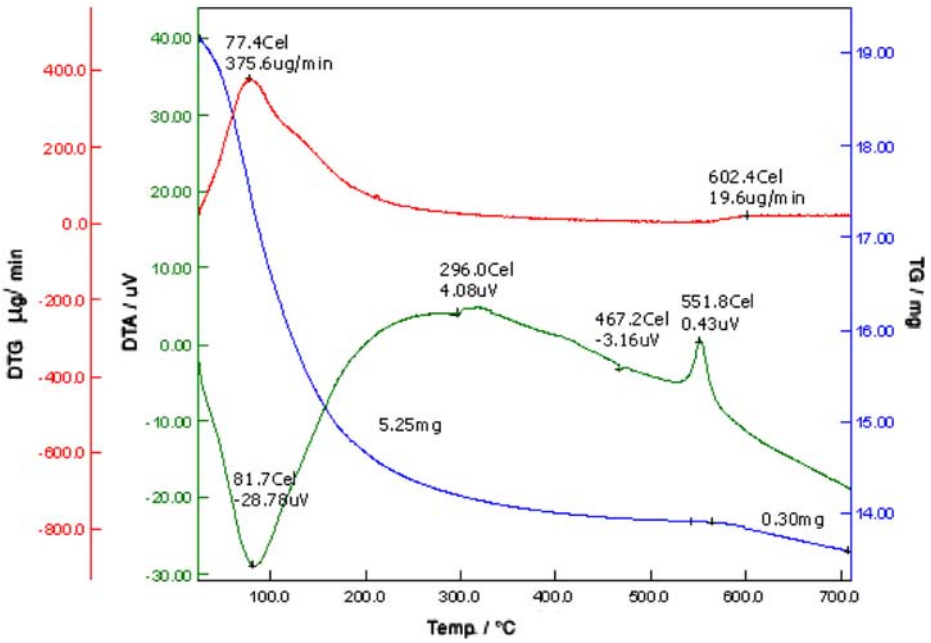

Fig. 1 DTG/DTA/TGA curves of sulfated $Zr(OH)_4$ sample

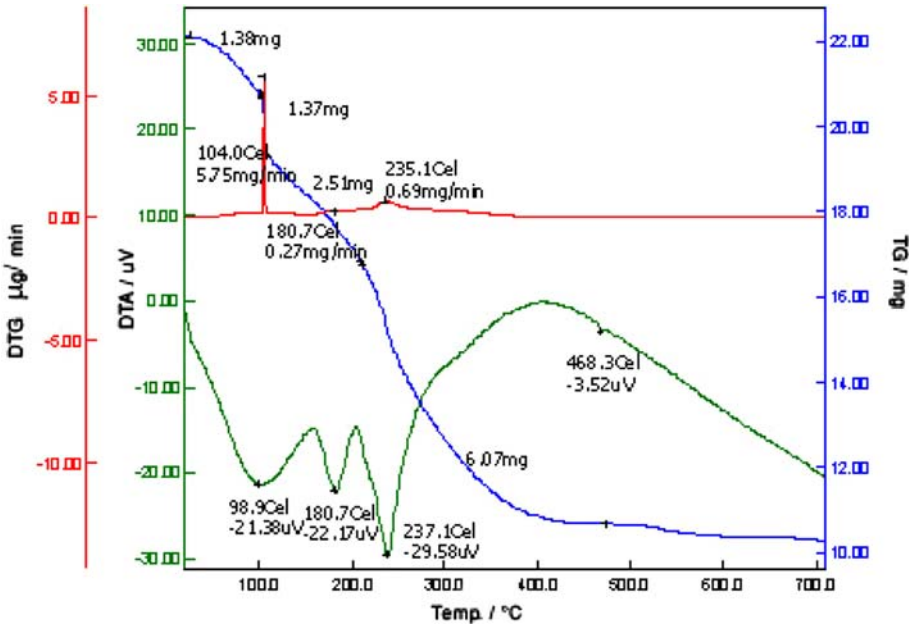

Fig. 2 DTG/DTA/TGA curves of Al^{3+}-sulfated $Zr(OH)_4$ sample

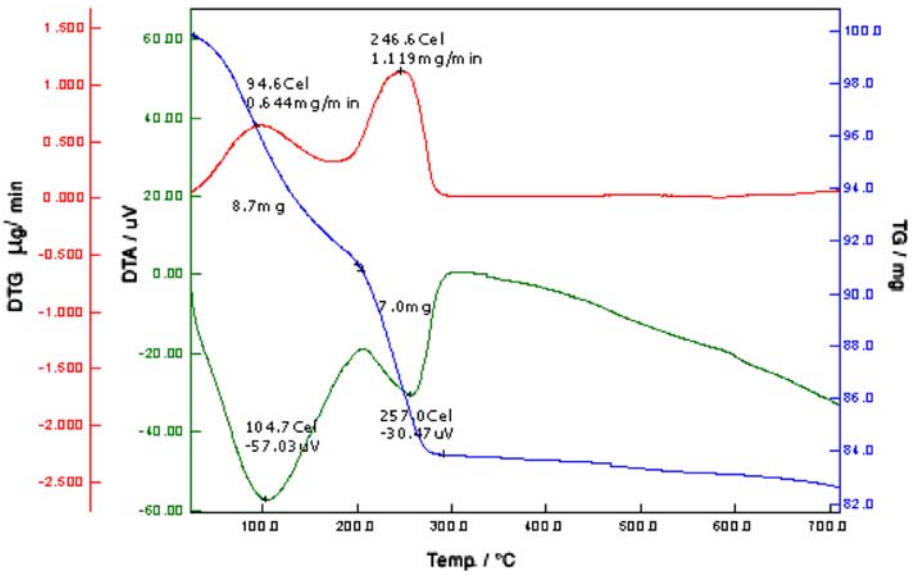

Fig. 3 DTG/DTA/TGA curves of sulfated $Sn(OH)_4$ sample

X-ray diffraction

Figure 4 shows XRD patterns of some of the catalysts investigated. The X-ray diffractograms of 550 °C calcination products reveal that all patterns are characteristic of pure SnO_2 phase with tetragonal cassiterite structure at 2θ of 26.54°, 33.82°, and 51.74° (JCPDS No. 41-1445). As indicated from the calculated crystal size using the Scherer equation (listed in Table 1), the intensities of the bands characteristic of cassiterite SnO_2 gradually decrease on increasing the sulfate content. A crystallite size of 102.8 nm was calculated from the broadening of the strongest main peak of SnO_2 at 2θ of 51.74°, and addition of sulfate was associated with a continuous decrease of crystallite size. This may be attributed to retardation of the crystal growth of SnO_2 on incorporation of sulfate groups [52–54]. In other words, the presence of sulfate groups on the surface of SnO_2 particles prevents their agglomeration during calcination [55]. The rise of calcination temperature was associated with narrowing of the XRD lines, indicating an increase of crystallite size and suggesting the sintering of crystalline SnO_2 [56], thus agreeing with the determined surface areas.

XRD patterns of calcined sulfated zirconium oxide show the presence of an intense peak at $2\theta = 30.253°$ and other less intense peaks at 35.23°, 50.628°, and 59.961°, characteristic of a tetragonal structure. During heating from 400 to 700 °C a substantial amount of sulfate is

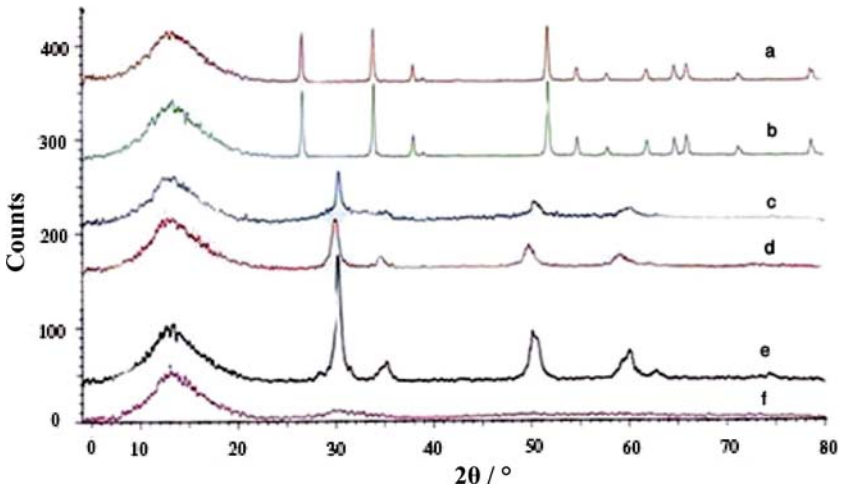

Fig. 4 XRD patterns of some investigated samples, *a* 10S/SnO_2—400 °C, *b* 10S/SnO_2—550 °C, *c* SZ—550 °C, *d* 5Al/SZ—550 °C, *e* 10Al/SZ—550 °C and *f* 15Al/SZ—400 °C

Table 1 Crystal size of the samples investigated

Samples	Crystal size (nm)	Samples	Crystal size (nm)
1Al/SZ	12	5S/SnO_2	87
5Al/SZ	16	10S/SnO_2	83
10Al/SZ	21	15S/SnO_2	79
15Al/SZ	27	20S/SnO_2	54.4
20Al/SZ	32		

decomposed, resulting in crystalline ZrO_2. The samples calcined at 400 °C are mainly amorphous. For the sample calcined at 550 °C the predominant phase is the tetragonal phase. As a result, introduction of different amounts of aluminum seems to have a positive effect on the crystal growth of ZrO_2 crystallites modifying the final oxide phase [57]. It is worth mentioning that the investigated XRD patterns of the Al/ZS system do not exhibit diffraction lines of Al_2O_3 phases, indicating they are present below the lowest concentration required for XRD detection.

Surface-area measurement

The different surface characteristics of the investigated catalysts calcined at 400 °C were determined from nitrogen adsorption isotherms obtained at −196 °C. These characteristics include the specific surface area S_{BET}, total pore volume (V_T), and mean pore diameter (d). The data obtained are listed in Table 2. The adsorption isotherms are of type IV of BDDT classifications [58].

It can be seen from Table 2 that Al/SZ samples exhibit a decrease of surface areas with increasing amounts of incorporated Al_2O_3. This decrease in N_2-S_{BET} may be attributed to impregnation inside the pores resulting in a decrease in the total pore volume V_T [36, 60, 61]. In addition, it should be noted that the decrease in specific surface area was accompanied by an increase in the mean pore diameter.

For S/SnO_2, on the other hand, an increase of sulfate content is associated with a continuous increase of surface area. It is clear that the interaction between SO_4^{2-} and SnO_2 stabilizes the SnO_2 against sintering, producing a thermally stable cassiterite structure. In other words, sulfate anions on the surface of SnO_2 can effectively impede its crystallization, thus hindering the loss of its surface area [59].

Acidity measurement

The surface acidity of the samples was been evaluated using different methods as discussed below:

(i) Potentiometric titration curves using *n*-butylamine as a probe molecule in non-aqueous media enabled estimation of the relative strength. Sharma et al. and

Table 2 Textural data for the catalysts investigated

Samples	S_{BET} ($m^2\ g^{-1}$)	V_T ($cm^3\ g^{-1}$)	d (nm)	Samples	S_{BET} ($m^2\ g^{-1}$)	V_T ($cm^3\ g^{-1}$)	d (nm)
1Al/SZ	191.7	0.3512	7.33	5S/SnO_2	7.9	0.0564	28.55
5Al/SZ	128	0.0.291	9.1	10S/SnO_2	9.65	0.0630	26.11
10Al/SZ	125.8	0.3150	10.02	15S/SnO_2	21.3	0.0986	18.52
15Al/SZ	109.4	0.3009	11.0	20S/SnO_2	32.8	0.1249	15.23
20Al/SZ	92.9	0.2857	12.3	30S/SnO_2	42.18	0.1530	14.51

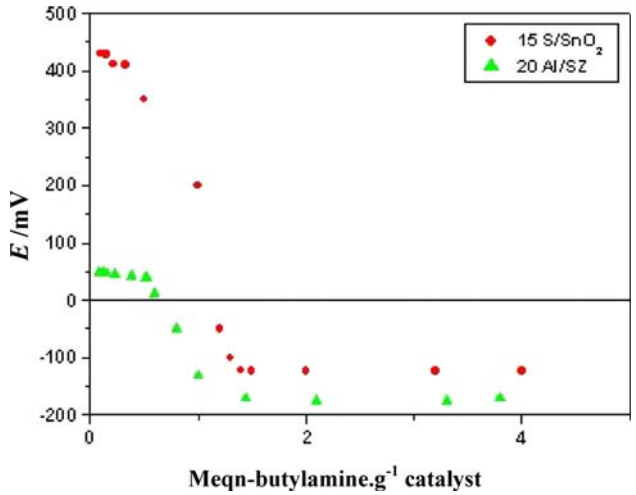

Fig. 5 Potentiometric titration curves for evaluating acid strength

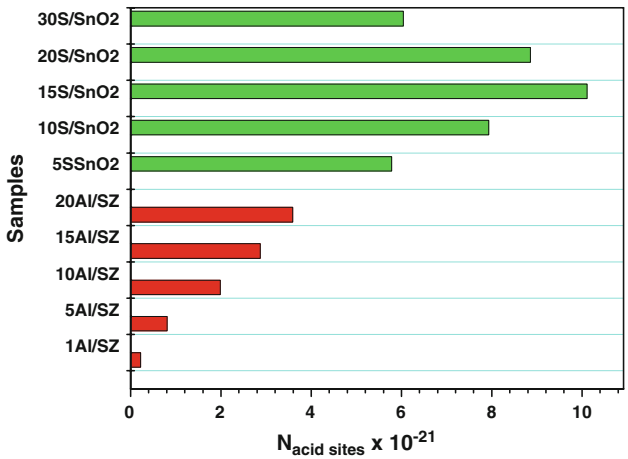

Fig. 6 Total acidities of the samples investigated

Cid and Pecci [62, 63] have reported an approximate scale on which the measured initial potential E_i may be used to indicate acid strength, i.e., $E_i > 100$ mV (very strong sites), $0 < E_i < 100$ mV (strong sites), $-100 < E_i < 0$ (weak sites), and $E_i < -100$ mV (very weak sites). Figure 5 shows representative potentiometric titration curves of some of the catalysts investigated, where the point at which no further change of electrode potential occurs enables calculation of the total number of acid sites. It is evident that S/SnO_2 measures the highest value of E_i, whereas Al/SZ measures the lowest value of E_i. This indicates that the strength of the acid sites of S/SnO_2 is higher than the strength of those of Al/SZ.

(ii) Thermogravimetric analysis (TGA) of adsorbed pyridine is a convenient and promising technique for estimating the number of acid sites and determining their relative strengths. The total numbers of acid sites of investigated samples is presented in Fig. 6. Inspection of Fig. 6 reveals that:

a. A preliminary test carried out to study the effect of calcination temperature on the acylation of toluene using $10S/SnO_2$ and 20Al/SZ indicated that samples calcined at 550 °C had the highest acidity and relatively higher acidic strength than those calcined at 400 and 700 °C. The lower acidity of the 400 °C calcination product may be judged from the difficult interaction of SO_4^{2-} with the oxide surface to form strong acid sites [64]. On the other hand, elevation of the calcination temperature to 700 °C leads to the hydrolytic dissociation of surface acidic groups and removal of sulfate groups, leading to the ultimate formation of SO_3 moieties [18, 65, 66].

b. Incorporation of SO_4^{2-} into SnO_2 was accompanied by a gradual increase of both total number and strength of acid sites to reach a maximum at an SO_4^{2-} loading of 15 wt%. This means that the distribution and number of sulfate groups on the surface of SnO_2 approaches a maximum and is responsible for the higher acidity, including Lewis and Bronsted acidity, for 550 °C calcination products. The potentiometric titration indicates that SO_4^{2-}/SnO_2 catalysts could be solid superacids similar to other sulfated metal oxides [32, 33]. The acidity of the SO_4^{2-}/metal oxide arises from the nature of S=O in the complex formed by interaction of SO_4^{2-} with the metal oxide surface and the inductive effect caused by S=O groups in the complex [67, 68].

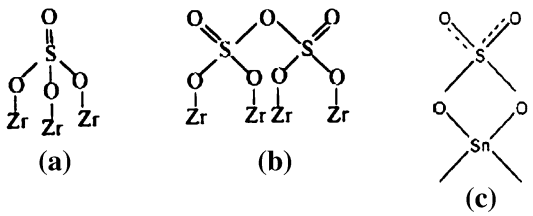

c. The incorporation of Al_2O_3 into SZ samples increases the Bronsted and Lewis surface acidity on increasing the metal oxide content. The ratio of Bronsted/Lewis acid sites (B/L) for Al/SZ affects the acylation reaction to different extents.

(iii) FT-IR spectra of pyridine adsorbed on samples calcined at 550 °C are shown in Fig. 7. FT-IR spectra of unmodified SnO_2 show a Lewis acid site band at 1,445 cm^{-1} and a very weak Bronsted acid site band at 1,541 cm^{-1}. Addition of sulfate was accompanied by enhancing of surface acidity, namely the Lewis and Bronsted acid sites [69]. FT-IR spectra of sulfated tin oxide exhibits several

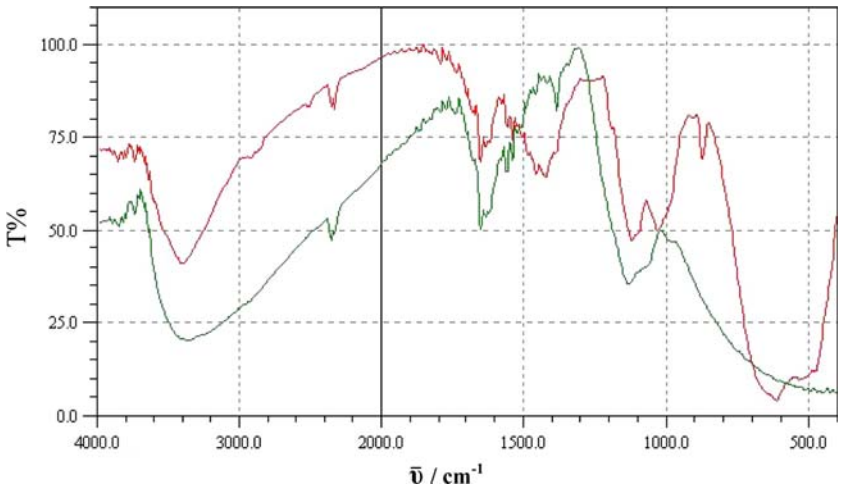

Fig. 7 FT-IR spectra of pyridine adsorbed on samples calcined at 550 °C

bands, namely at 1,450 and 1,537 cm^{-1}, attributed to the chemisorbed pyridine on Lewis acid sites and Bronsted acid sites, respectively. The bands assigned at 1,610 and 1,633 cm^{-1} may be attributed to pyridine chemisorbed on Lewis acid sites whereas the band at 1,485 cm^{-1} is assigned to pyridine chemisorbed on either Lewis or Bronsted acid sites. FT-IR bands within the range 1,112−1,136 cm^{-1} may be characteristic of bidentate sulfate [65].

Incorporation of Al_2O_3 into SZ samples results in a different FT-IR pattern, mainly the ratio of B/L bands, with a slight shift of the bands corresponding to both Lewis and Bronsted acid sites, therefore agreeing with their lower efficiency for acylation of toluene.

Catalytic activity measurements

Friedel–Crafts acylation of toluene using the investigated samples gives a mixture of *p*-methylacetophenone as a major product and *o*-methylacetophenone as a minor product. The *p* isomer is favored because of its lower energy and the lowest steric hindrance between the methyl group and the entering acetyl group. Depicted in Fig. 8 is the yield of the acylation product mixture (*o* and *p*-methylacetophenone) using 550 °C calcination products.

Inspection of Fig. 8 reveals that:

(i) Sulfated SnO_2 is the most promising Friedel–Crafts acylating catalyst. The catalytic acylation of toluene into *o* and *p*-methylacetophenone increases on increasing the sulfate content up to 10 wt% whereas further increase of sulfate beyond 10 wt% is associated with a decrease of the catalytic activity. Good agreement was observed between acylation activity and the total number of acid sites and their strength.

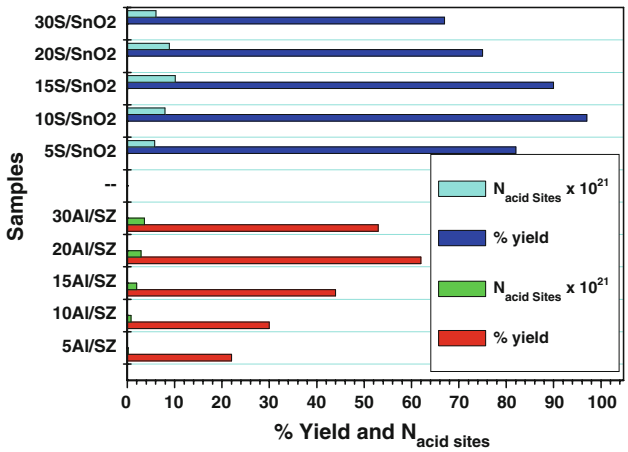

Fig. 8 Correlation between the catalyst composition, $N_{acid\ sites}$, and yield of *o*- and *p*-methylacetophenone

(ii) Incorporation of Al_2O_3 into sulfated zirconia results in lower efficiency in the acylation of toluene in solvent-free medium. The efficiency is even lower than that of all the sulfated tin oxides. This may be attributed to the lower surface acidity of Al/SZ compared with S/SnO_2, and the ratio of B/L for sulfated zirconia with incorporated Al_2O_3 is much higher than that of sulfated tin oxide.

Preliminary Friedel–Crafts experiments were performed to study the efficiency of $10/SnO_2$, the most efficient and promising catalyst, in the acylation of benzene derivatives. It was observed that anisole is the most active substrate in acylation with acetic acid anhydride (98% yield) whereas chlorobenzene and nitrobenzene are less active (48 and 19% yield, respectively). The lower activity of nitrobenzene is attributed to deactivation of the aromatic ring by the $–NO_2$ substituent, indicating that harsher conditions are required to drive the reaction to completion.

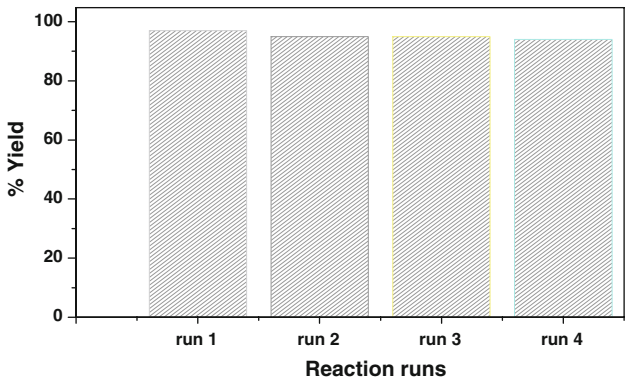

Fig. 9 Reusability of $10S/SnO_2$ in the acylation of toluene

Reusability investigation

Recycling of the catalyst is an important aspect of an industrial process. For this purpose, reusability of the catalyst was tested by carrying out repeated runs of the reaction at 70 °C, using the most efficient catalyst, $10S/SnO_2$, and keeping the mixture of reactants (toluene–acetic anhydride) at 15:10 cm^3, respectively. After performing the reaction over fresh catalyst, the catalyst was reactivated with N_2 at 300 °C for 3 h. The reaction was again conducted on the reactivated catalyst at 70 °C. It is evident fron Fig. 9 that the activity of the catalyst did not decrease notably even after four cycles.

Conclusions

The incorporation of sulfates into zirconia samples enhances the thermal stability of amorphous zirconia. The samples contain mixtures of monoclinic and tetragonal zirconia phases, but the 550 °C calcination products contain a maximum of the tetragonal phase.

The incorporation of Al^{3+} into SZ samples enhances the crystallinity of the samples, and the impregnation occurs inside the pores, causing, therefore, a continuous decrease of surface area. It is worth mentioning that introduction of Al^{3+} into SZ was associated with a continuous increase of surface acidity, namely Bronsted/Lewis acidity, and therefore lower activity in the acylation of toluene.

Addition of sulfate to SnO_2 leads to a continuous decrease of crystallite size, because crystal growth of SnO_2 is retarded by prevention of agglomeration during calcination. Increasing the amount of SO_4^{2-} is therefore accompanied by an increase of S_{BET}-N_2.

Sulfation of tin oxide creates new acid sites where Lewis/Bronsted acidity exceeds that of sulfated zirconia. Moreover, the strength of acid sites of SO_4^{2-}/SnO_2 is the highest, giving therefore higher yields of toluene acylation products.

Experimental

Preparation of the catalysts

For preparation of tin oxide gel used as a precursor of SO_4^{2-}/SnO_2, 23.3 g crystallized $SnCl_4{\cdot}5H_2O$ was dissolved in 2 dm^3 distilled water followed by the dropwise addition of concentrated aqueous ammonia to form a precipitate until the pH was approximately 8. The white precipitate obtained was filtered and washed thoroughly with 2% CH_3COONH_4 solution until all chloride was eliminated (silver nitrate test). The $Sn(OH)_4{\cdot}XH_2O$ gels were placed in appropriate amounts of 1 M H_2SO_4 solution to furnish 5, 10, 15, 20, and 30 wt% sulfates. These gels were dried at 100 °C for 24 h, followed by calcination at 550 °C for 8 h.

Zirconium hydroxide as received from Sigma–Aldrich was soaked in H_2SO_4 to prepare 20 wt% sulfate in SO_4^{2-}/ZrO_2. The resulting suspension was dried on a water bath with constant stirring. All prepared samples were dried at 120 °C overnight and then calcined in air at 550 °C for 8 h.

Zirconium(IV) hydroxide containing 20 wt% SO_4^{2-} was prepared and soaked in $Al(NO_3)_3{\cdot}9H_2O$ to prepare 5, 10, 15, 20, and 30 wt% Al_2O_3 in Al_2O_3–SO_4^{2-}/ZrO_2. The resulting suspension was dried on a water bath with constant stirring. All prepared samples were dried at 120 °C overnight and then calcined in air at 550 °C for 8 h.

Catalyst characterization

Thermal analysis (DTA, TGA, DTG) of the uncalcined samples were carried out using a Shimadzu type 50-H thermal analyzer. The samples under examination were heated in an N_2 stream at a rate of 10 °/min.

The powder diffraction patterns were recorded on a PW 150 (Philips) X-ray powder diffractometer (XRD) using Ni filtered Cu Kα radiation ($\lambda = 1.540$ Å) at 40 kV, 30 mA, and a scanning range 2θ of 18−80°. The crystallite size (nm) was calculated from the broadening of the strongest peak of the respective XRD, using the Scherrer equation:

$$D = k\lambda/(\beta \cos\theta)$$

where k is the crystallite shape constant (≈ 1), λ is the radiation wavelength (Å), β is the line width (radians), and θ is the Bragg angle.

The specific surface areas of the calcined samples were determined from a nitrogen adsorption study conducted at −196 °C using the high-vacuum conventional volumetric glass system. Prior to any adsorption measurement the sample was degassed at 200 °C for 2 h under a reduced pressure of 10^{-5} Torr.

Surface acidity measurements

Surface acidity measurements of the precalcined investigated catalysts were performed using three different methods as described below:

(i) The acid strength of the solid samples was determined using potentiometric titration [45, 46]. The solid (0.05 g) was suspended in 10 cm^3 acetonitrile (Sigma–Aldrich) and agitated for 3 h, while the suspension was titrated by addition of 0.1 N *n*-butylamine in acetonitrile (0.05 cm^3/min). Electrode potential variation was measured with an Orion model 420 A digital meter and a double-junction electrode.

(ii) Lewis and Bronsted acid sites on the surface were assigned by FT-IR spectroscopy of adsorbed pyridine. Prior to pyridine adsorption [46], the samples were activated at 200 °C for 3 h, followed by soaking in dry pyridine. Excess pyridine was then removed by evaporation. FT-IR spectra of the samples were acquired with a Shimadzu FT-IR spectrophotometer by mixing 0.005 g sample with 0.100 g KBr in 30 mm diameter self-supporting disks.

(iii) For 550 °C calcination products pre-exposed to pyridine the relative acid strength and the amounts of acid were determined by thermal analysis (DSC, TGA). Prior to analysis, the samples were activated at 120 °C for 2 h to remove physisorbed water and pyridine. DSC and TGA scans were then carried out on the samples with a scan rate of 3 °/min up to 600 °C.

Catalytic activity measurements

Catalytic acylation of toluene was performed at atmospheric pressure in a batch-type reactor consisting of a round-bottomed flask equipped with a condenser, heated using a heating mantle. A typical reaction was carried out by adding 15 cm^3 toluene and 10 cm^3 acetic anhydride to 0.5 g fresh catalyst, and the reaction temperature was adjusted to 70 °C by use of the heating mantle.

Acknowledgments Financial support (project number 8058) by the deanship of scientific research at King Faisal University is gratefully acknowledged.

References

1. Olah GA (1973) Friedel-Crafts Chemistry. Wiley, New York
2. Franck GG, Stadelhofer JW (1988) Industrial aromatic chemistry. Springer Verlag, Berlin
3. Signoretto M, Torchiaro A, Breda A, Pinna F, Cerrato G, Morterra C (2008) Appl Catal B 84:363
4. Rohan D, Cnaff C, Formentin E, Guisnet M (1998) J Catal 177:296
5. Choudary BM, Sateesh M, Kantam ML, Prasad KVR (1998) Appl Catal A 171:155
6. Garg S, Soni K, Kumaran GM, Bal R, Gora-Marek K, Gupta JK, Sharma LD, Dhar GM (2009) Catal Today 141:125
7. El-Sharkawy EA, Al-Shihry SS (2004) Mater Lett 58:2122
8. Khder AS, El-Sharkawy EA, El-Hakam SA, Ahmed AI (2008) Catal Commun 9:769
9. Braga VS, Barros ICL, Garcia FAC, Dias FCL, Dias JA (2008) Catal Today 133:106
10. Hino M, Arata K (1980) J Chem Soc Chem Commun 851
11. Yamaguchi T (1990) Appl Catal A 61:1
12. Arata K (1990) Adv Catal 37:165
13. Shiju NR, Guliantsa VV (2009) Appl Catal A 356:1
14. Clark JH, Monks GL, Nightingale DJ, Price PM, White JF (2000) J Catal 193:348
15. Yadav GD, Goel PK, Joshi AV (2001) Green Chem 3:92
16. Arata K, Nakamura H, Shouji M (2000) Appl Catal A 197:213
17. Deutsch J, Prescott H, Muller D, Kemnitz E, Lieske H (2005) J Catal 231:269
18. El-Sharkawy EA, El-Hakam SA, Samra SE (2000) Mater Lett 42:331
19. Chen CL, Cheng S, Lin HP, Wong ST, Mou CY (2001) Appl Catal A 215:21
20. Xia QH, Hidajat K, Kawi S (2002) J Catal 205:318
21. Sun YY, Zhu L, Lu HJ, Wang RW, Lin S, Jiang DZ, Xiao FS (2002) Appl Catal A 237:21
22. Ghedini E, Signoretto M, Pinna F, Cerrato G, Morterra C (2006) Appl Catal B 67:24
23. Harmer MA, Sun Q, Vega AJ, Farneth WE, Heidekum A, Hölderich WF (2000) Green Chem 2:7
24. Martínez F, Morales G, Martín A, van Grieken R (2008) Appl Catal A 347:169
25. Liu Y, Xu L, Xu B, Li Z, Jia L, Guo W (2009) J Mol Catal 297:86
26. Hino M, Arata K (1999) React Kinet Catal Lett 66:331
27. Hino M, Arata K (1996) Catal Lett 34:125
28. Patil PT, Malshe KM, Kumar P, Dongare MK, Kemnitz E (2002) Catal Commun 3:411
29. Corma H, Garcia H (2003) Chem Rev 103:4307
30. Olah GA (1963) Friedel−Crafts and related reactions, vols 1−4. Wiley, New York, London
31. Olah GA, Prakash GKS, Sommer J (1985) Superacids, vols 1−4. Wiley, New York, Brisbane, Toronto
32. Matsuhashi H, Miyazaki H, Arata K (2001) Chem Lett 5:452
33. Matsuhashi H, Miyazaki H, Kawamura Y, Nakamura H, Arata K (2001) Chem Mater 13:3038
34. Hino M, Kurashige M, Matsuhashi H, Arata K (2006) Thermochim Acta 441:35
35. Bensi HA (1957) J Phys Chem 61:970
36. El-Sharkawy EA, Mostafa MR, Youssef AM (1999) Colloids Surf A 157:211
37. Dragoi B, Gervasini A, Dumitriu E, Auroux A (2004) Thermochim Acta 420:127
38. Mohamed MM, Abu-Zied BM (2000) Thermochim Acta 359:109
39. Wang WJ, Chen YW (1991) Catal Lett 10:297
40. Furuta S, Matsuhashi H, Arata K (2004) Appl Catal A 269:187
41. Tanabe K, Masui S, Nishizaki T (1970) J Res Inst Catal Hokkaido Univ 19:1
42. Corma A, Rodellas C, Fornes V (1984) J Catal 88:374
43. El-Sharkawy EA (1998) Adsorpt Sci Technol 16:193
44. Guo HF, Yan P, Hao XY, Wang ZZ (2008) Mater Chem Phys 112:1065
45. Hill CI (1998) Chem Rev 98:1
46. Matsuhashi H, Motoi H, Arata K (1994) Catal Lett 26:325
47. Scurrell MS (1987) Appl Catal 34:109

48. Srinivasan R, Toulbee D, Davis BH (1991) Catal Lett 9:1
49. Wang X, Xie Y (2001) React Kinet Catal Lett 72:115
50. Patel A, Coudurier G, Essayem N, Vedrine JC (1997) J Chem Soc Faraday Trans 93:347
51. Arata K (1990) Adv Catal 37:165
52. Hino M, Arata K (1979) Chem Lett 1259
53. Hino M, Arata K (1979) Chem Commun 1148
54. Hino M, Arata K (1979) J Am Chem Soc 101:6439
55. Jogalekar AY, Jaiswal RG, Jayaram RV (1998) J Chem Technol Biotechnol 71:234
56. Zhang J, Gao L (2004) J Solid State Chem 177:1425
57. Canton P, Olindo R, Pinna F, Strukul G, Piello P, Meneghetti M, Cerrato G, Mortera C, Benedetti A (2001) Chem Mater 13:1634
58. Brunauer S, Deming LS, Deming WE, Teller E (1940) J Am Chem Soc 62:1723
59. Gutierrez-Baez R, Toledo-Antonio JA, Cortes-Jacome MA, Sebastian PJ, Vazques A (2004) Langmuir 20:4265
60. El-Sharkawy EA, Al-Shihry SS, Ahmed AI (2003) Adsorpt Sci Technol 21:863
61. El-Sharkawy EA (2006) Monatsh Chem 137:1487
62. Sharma P, Vyas S, Patel A (2004) J Mol Catal 214:281
63. Cid R, Pecci G (1985) Appl Catal A 14:15
64. Sun Y, Zhu L, Lu H, Wang R, Lin S, Jiang O, Xiao FS (2002) Appl Catal A 237:21
65. Mishra HK, Parida KM (2002) Appl Catal A 224:179
66. Tran MT, Gnep NS, Szabo G, Guisnet M (1998) Appl Catal A 171:207
67. Tanabe K, Misono M, Ono Y, Hattori H (1989) New solid acids and bases (Chapter 4). Elsevier Science, Amsterdam
68. Sohn JR, Lee SH (2004) Appl Catal A 266:89
69. Sakthivel R, Prescott HA, Deutsch J, Lieske H, Kemnitz E (2003) Appl Catal A 253:237